REPORT DOCUMENTATION PAGE

Form Approved OMB NO. 0704-0188

1. REPORT DATE (DD-MM-YYYY)	2. REPORT TYPE	3. DATES COVERED (From - To)
15-05-2010	Final Report	15-Sep-2006 - 14-Sep-2009

4. TITLE AND SUBTITLE

Final Report: Spectroscopy of Many-Body Effects in Carbon Nanotubes

5a. CONTRACT NUMBER

W911NF-06-1-0376

5b. GRANT NUMBER

5c. PROGRAM ELEMENT NUMBER

611102

6. AUTHORS

Junichiro Kono

5d. PROJECT NUMBER

5e. TASK NUMBER

5f. WORK UNIT NUMBER

7. PERFORMING ORGANIZATION NAMES AND ADDRESSES

William Marsh Rice University
William Marsh Rice University
6100 Main
Houston, TX 7725 -1182

8. PERFORMING ORGANIZATION REPORT NUMBER

9. SPONSORING/MONITORING AGENCY NAME(S) AND ADDRESS(ES)

U.S. Army Research Office
P.O. Box 12211
Research Triangle Park, NC 27709-2211

10. SPONSOR/MONITOR'S ACRONYM(S)

ARO

11. SPONSOR/MONITOR'S REPORT NUMBER(S)

49735-PH.1

12. DISTRIBUTION AVAILIBILITY STATEMENT

Approved for Public Release; Distribution Unlimited

13. SUPPLEMENTARY NOTES

The views, opinions and/or findings contained in this report are those of the author(s) and should not contrued as an official Department of the Army position, policy or decision, unless so designated by other documentation.

14. ABSTRACT

The goal of this research project was to explore the fundamental properties of degenerate one-dimensional (1-D) electrons in single-walled carbon nanotubes (SWNTs) using dynamical methods to probe and understand electronic correlations and many-body phenomena. We studied two aspects of 1-D electron correlations in SWNTs: Fermi-edge singularities (FES) and conduction electron spin resonance (ESR). For the FES project, three major strides were taken: first, a detailed design of the carbon nanotube field effect transistor structure was made, and a

15. SUBJECT TERMS

carbon nanotubes, many-body effects, spin resonance, Fermi-edge singularities

16. SECURITY CLASSIFICATION OF:			17. LIMITATION OF ABSTRACT	15. NUMBER OF PAGES	19a. NAME OF RESPONSIBLE PERSON
a. REPORT	b. ABSTRACT	c. THIS PAGE			Junichiro Kono
UU	UU	UU	UU		19b. TELEPHONE NUMBER 713-348-2209

Report Title

Final Report: Spectroscopy of Many-Body Effects in Carbon Nanotubes

ABSTRACT

The goal of this research project was to explore the fundamental properties of degenerate one-dimensional (1-D) electrons in single-walled carbon nanotubes (SWNTs) using dynamical methods to probe and understand electronic correlations and many-body phenomena. We studied two aspects of 1-D electron correlations in SWNTs: Fermi-edge singularities (FES) and conduction electron spin resonance (ESR). For the FES project, three major strides were taken: first, a detailed design of the carbon nanotube field effect transistor structure was made, and a step-by-step procedure was followed for fabrication; second, micro-photoluminescence was performed on individual SWNTs in the presence of external electric fields; and third, we made the first direct observation of "dark" excitons in individual SWNTs through low-temperature micro-magneto-photoluminescence spectroscopy. The ESR project has broken new ground on our current understanding of spin resonance in SWNTs. Last year, we discovered that oxygen plays a key role in the electron spin dynamics in nanotubes. Comparing temperature dependent ESR data taken on the same nanotube film in the water-free condition and in the water-free and oxygen-free condition, we were able to perform a detailed lineshape analysis. Several new observations resulted, including an increase in the spin susceptibility when oxygen is removed, Curie-law behavior for the water-free spin susceptibility, linewidth motional narrowing, and saturation of the absorption curve at high microwave powers. In addition, work has begun on producing sample configurations for the single-tube ESR experiment.

List of papers submitted or published that acknowledge ARO support during this reporting period. List the papers, including journal references, in the following categories:

(a) Papers published in peer-reviewed journals (N/A for none)

A. Srivastava, H. Htoon, V. I. Klimov, and J. Kono, "Direct Observation of Dark Excitons in Individual Carbon Nanotubes: Inhomogeneity in the Exchange Splitting," Physical Review Letters 101, 087402 (2008).

Number of Papers published in peer-reviewed journals: 1.00

(b) Papers published in non-peer-reviewed journals or in conference proceedings (N/A for none)

Number of Papers published in non peer-reviewed journals: 0.00

(c) Presentations

J. Kono, “Low-Energy Dynamics in Single-Walled Carbon Nanotubes,” Electrochemical Society 217th Meeting, H3 - Carbon Nanotubes and Nanostructures: Fundamental Properties and Processes Sessions, Vancouver, Canada, April 25-30, 2010.

J. Kono, “Dynamics of One-Dimensional Electrons, Phonons, and Excitons in Carbon Nanotubes,” Condensed Matter Seminar, Department of Physics, Texas A&M University, March 31, 2010.

J. Kono, “Electronic Structure and Dynamics in Single-Walled Carbon Nanotubes,” Gordon Conference on Ultrafast Phenomena in Cooperative Systems, Galveston, Texas, February 28 – March 5, 2010.

J. Kono, “Spectroscopy of Carbon Nanotubes: Correlations, Quantum Coherence, and Many-Body Effects,” Seminar, Institute of Physics, Chinese Academy of Sciences, Beijing, China, October 19, 2009.

J. Kono, “Low-Energy Dynamics in Single-Walled Carbon Nanotubes,” 2009 Hangzhou Workshop on Quantum Matter, Zhejiang University, Hangzhou, China, October 12-15, 2009.

J. Kono, “Low-Energy Dynamics in Carbon Nanotubes,” Fourteenth International Conference on Narrow Gap Semiconductors (NGS-14), Sendai, Japan, July 13-17, 2009.

J. Kono, “Terahertz Dynamics in Carbon Nanotubes,” Third International Workshop on Nanotube Optics and Nanospectroscopy (WONTON 09), Matsushima, Japan, June 7-10, 2009.

J. Kono, “Dynamics of One-Dimensional Electrons, Phonons, and Excitons in Carbon Nanotubes,” Seminar, Osaka University, Osaka, Japan, February 27, 2009.

W. D. Rice, R. Weber, A. Leonnard, A.-L. Tsai, and J. Kono, “Temperature Dependence of Electron Spin Dynamics in Oxygen-Free Single-Walled Carbon Nanotubes” (oral), 2010 March Meeting of the American Physical Society, Seattle, Washington, March 15-19, 2010.

W. D. Rice and J. Kono, “Electron Spin Resonance in Single-Walled Carbon Nanotubes” (oral), 2008 March Meeting of the American Physical Society, New Orleans, Louisiana, March 10-14, 2008.

W. D. Rice, M. Fabian, Q. Si, and J. Kono, “Electron Paramagnetic Resonance of Single-Walled Carbon Nanotubes” (poster), The International Conference on Strongly Correlated Electron Systems, Houston, Texas, May 13-18, 2007.

Number of Presentations: 11.00

Non Peer-Reviewed Conference Proceeding publications (other than abstracts):

Number of Non Peer-Reviewed Conference Proceeding publications (other than abstracts): 0

Peer-Reviewed Conference Proceeding publications (other than abstracts):

Number of Peer-Reviewed Conference Proceeding publications (other than abstracts): 0

(d) Manuscripts

Number of Manuscripts: 0.00

Patents Submitted

Patents Awarded

Graduate Students

NAME	PERCENT_SUPPORTED
William D. Rice	0.50
Ajit Srivastava	0.50
Yang Li	0.50
FTE Equivalent:	**1.50**
Total Number:	**3**

Names of Post Doctorates

NAME	PERCENT_SUPPORTED
FTE Equivalent:	
Total Number:	

Names of Faculty Supported

NAME	PERCENT_SUPPORTED	National Academy Member
Junichiro Kono	0.08	No
FTE Equivalent:	**0.08**	
Total Number:	**1**	

Names of Under Graduate students supported

NAME	PERCENT_SUPPORTED
FTE Equivalent:	
Total Number:	

Student Metrics

This section only applies to graduating undergraduates supported by this agreement in this reporting period

The number of undergraduates funded by this agreement who graduated during this period:	0.00
The number of undergraduates funded by this agreement who graduated during this period with a degree in science, mathematics, engineering, or technology fields:.....	0.00
The number of undergraduates funded by your agreement who graduated during this period and will continue to pursue a graduate or Ph.D. degree in science, mathematics, engineering, or technology fields:.....	0.00
Number of graduating undergraduates who achieved a 3.5 GPA to 4.0 (4.0 max scale):	0.00
Number of graduating undergraduates funded by a DoD funded Center of Excellence grant for Education, Research and Engineering:	0.00
The number of undergraduates funded by your agreement who graduated during this period and intend to work for the Department of Defense	0.00
The number of undergraduates funded by your agreement who graduated during this period and will receive scholarships or fellowships for further studies in science, mathematics, engineering or technology fields:	0.00

Names of Personnel receiving masters degrees

NAME
William D. Rice
Total Number: 1

Names of personnel receiving PHDs

NAME
Ajit Srivastava
Total Number: 1

Names of other research staff

NAME	PERCENT_SUPPORTED
FTE Equivalent:	
Total Number:	

Sub Contractors (DD882)

Inventions (DD882)

PROJECT ACTIVITIES (September 15, 2006 – September 14, 2009)

ARO
(Contract No. W911NF-06-1-0376, J. Kono, Rice University)

Abstract:

The goal of this research project was to explore the fundamental properties of degenerate one-dimensional (1-D) electrons in single-walled carbon nanotubes (SWNTs) using dynamical methods to probe and understand electronic correlations and many-body phenomena. SWNTs are an ideal 1-D system for studying novel quantum effects in nanostructures. There have been transport and optical studies on SWNTs by a number of groups during the past decade, revealing some characteristic features of 1-D systems. However, most of the predicted exotic properties of interacting 1-D electrons are yet to be observed and some of the reported experimental evidence remains controversial. Here, we studied two aspects of 1-D electron correlations in SWNTs: Fermi-edge singularities (FES) and conduction electron spin resonance (ESR). We made significant progress and accomplishments on both projects during the last three years. For the FES project, three major strides were taken: first, a detailed design of the carbon nanotube field effect transistor structure was made, and a step-by-step procedure was followed for fabrication; second, micro-photoluminescence was performed on individual SWNTs in the presence of external electric fields; and third, we made the first direct observation of "dark" excitons in individual SWNTs through low-temperature micro-magneto-photoluminescence spectroscopy. The ESR project has broken new ground on our current understanding of spin resonance in SWNTs. Last year, we discovered that oxygen plays a key role in the electron spin dynamics in nanotubes. Comparing temperature dependent ESR data taken on the same nanotube film in the water-free condition and in the water-free and oxygen-free condition, we were able to perform a detailed lineshape analysis. Several new observations resulted, including an increase in the spin susceptibility when oxygen is removed, Curie-law behavior for the water-free spin susceptibility, linewidth motional narrowing, and saturation of the absorption curve at high microwave powers. In addition, work has begun on producing sample configurations for the single-tube ESR experiment.

Project 1: Fermi-Edge Singularities in Carbon Nanotubes

Introduction:

When a photon with energy greater than the band gap of a direct-gap semiconductor is absorbed, an electron-hole pair is formed inside the crystal. In low dimensional systems where the Coulomb interaction is not effectively screened, strongly Coulomb correlated electron-hole pair, or excitons, dominate optical spectra. In one-dimensional (1-D) systems such as SWNTs, excitons are predicted to be extremely stable, carrying nearly all of the oscillator strengths of interband optical transitions. In fact, in SWNTs it is now widely believed that such excitons determine the optical spectra of semiconducting nanotubes.

However, the situation is somewhat different in the case of a metallic or heavily doped semiconducting system possessing unipolar carriers (either *n*-type or *p*-type). At sufficiently low temperatures when $E_F >> k_B T$ so that the unipolar carrier system can be considered quantum degenerate, an electron-hole pair created by the photon is not an ordinary exciton but instead leads to the formation of a "many-body" exciton, or the Mahan exciton. For example, in the case of *n*-type carriers shown in Fig. 1, the photo-created hole in the valence band is correlated to not just one electron but to the whole Fermi sea in the conduction band (the case of *p*-type carriers is likewise). Due to many-body interactions among the electrons and between the electrons and the hole, strong scattering from the hole leads to power-law singularity known as the Fermi-edge singularity (FES) in the absorption and emission spectra. On the other hand, the orthogonal nature of the excited state containing the hole, with respect to the ground state, leads to a "shake up" process and the so-called Anderson Orthogonality Catastrophe, implying suppression of the singularity. Under most cases, the singularity dominates over the aforementioned catastrophe, thus making the observation of FES in optical spectroscopy experiments possible.

In 1-D systems, unlike 2-D and 3-D, theoretical predictions regarding observation of Fermi-edge singularities are somewhat conflicting, primarily due to the expected absence of a clear Fermi edge in a Tomonaga-Luttinger liquid (TLL). Some theoretical studies predict that TLL behavior should enhance this effect while others indicate that non-Fermi liquids cannot show any Fermi-edge singularities. However, recent theoretical studies predict power-law singularities even in TLLs with singularity exponents depending on the strength of interaction between the electrons, thus favoring the possibility of observing FES in 1-D systems like single-walled carbon nanotubes.

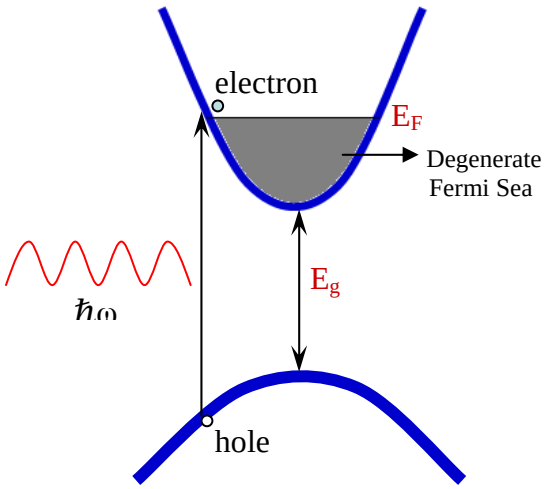

Figure 1. Illustration of Fermi-edge singularity in an *n*-doped degenerate semiconductor.

Fermi-edge singularities have been successfully observed in interband transitions in a variety of modulation-doped semiconductor quantum wells at low temperatures. However, experimental studies on modulation-doped semiconductor quantum wires have produced contradicting (and sometimes sample-dependent) results, and thus, no consensus has been achieved as to the appearance of FES in 1-D systems. Part of the problem is the small quantum

confinement in typical high-quality semiconductor quantum wire systems used in these studies, which makes it difficult or impossible to create a highly-degenerate electron system without populating the second subband. SWNTs, possessing much smaller diameters, can offer an interesting alternative to these previous studies.

In order to observe FES in SWNTs, we proposed to perform micro-photoluminescence (micro-PL) studies on individual semiconducting SWNTs at low temperatures as a function of temperature and gate voltage. For a systematic study of Fermi-edge singularities, we need to be able to change the Fermi level of a semiconducting nanotube in a controllable manner. This is possible through gating in carbon nanotube field effect transistors (CNT-FETs). Namely, in a CNT-FET, a semiconducting nanotube can be *n*-doped (or *p*-doped) to have a Fermi level inside the conduction band (or the valence band). As shown in Fig. 2, we plan to suspend a semiconducting nanotube over a trench, deposit electrodes on the ends and inside the trench to change the Fermi level. The suspended section of the nanotube serves as our sample and by changing the gate-voltage we can change the Fermi level to make it *n*- or *p*-doped. We can then measure micro-PL spectra of these samples as a function of gate voltage (or equivalently, carrier concentration) at low temperatures in a helium-flow microscopy cryostat. As the Fermi energy is increased by changing the gate voltage, it should be possible to systematically study the evolution of the many-body exciton from an ordinary exciton. It is expected that charged excitonic complexes like "trions" may form in the weak doping regime before many-body effects such as band-gap renormalization become important and finally lead to a degenerate quantum 1-D system. Thus, such a system is an ideal playground not only to study many-body physics in nanotubes, but also to study continuous evolution from two-body to many-body physics. This way we can hope to answer the question: "*How many is really many for many-body physics*?"

Accomplishments:

For an efficient execution of this project, we divided the whole project into different modules that were performed in parallel, and we made significant progress in all modules; i.e., i) a detailed design of the carbon nanotube field effect transistor structure is ready, ii) a step-by-step procedure was followed for fabrication; iii) micro-photoluminescence was performed on individual SWNTs in the presence of external electric fields; and iv) we made the first direct observation of "dark" excitons in individual SWNTs through low-temperature micro-magneto-photoluminescence spectroscopy. In the following, we explain our approach and provide a detailed report of our progress in various modules of this project:

Module 1. Fabrication of Carbon Nanotube Field Effect Transistor (CNTFET):

At the heart of this project lies the fabrication of CNTFET which enables us to controllably change the Fermi energy in a semiconducting nanotube by changing the gate voltage. By applying a positive bias to the gate, holes can be repelled from the nanotube, leading to *n*-doping. Similarly, *p*-doping can be achieved by applying a negative bias to the gate. As shown in Fig. 2, a nanotube bridges the trench, which we set to be 5-10 μm wide. We also set the depth of the trench to be 0.5-2 μm. We use the trench to inhibit the quenching of PL from the nanotube, which takes place when it touches the substrate. We deposit Au/Ti as pads to make the source and the drain electrodes. We use Mo/Fe or Co/Al as catalyst to do CVD so as to get nanotubes.

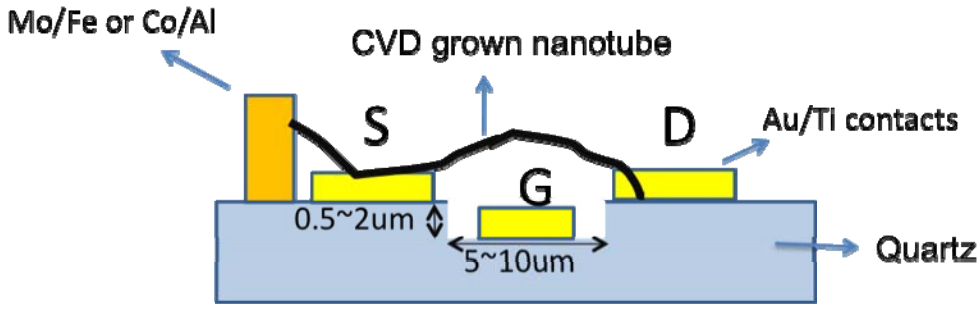

Figure 2. Schematic diagram of the CNTFET device.

We have a new design for the fabrication procedure of CNTFET with a step-by-step roadmap towards completion of the device. We use Rice University's class 1000 clean room for various photolithographic processes. We first made a photomask using the DWL66 Mask Maker in the clean room. This consisted of designing a mask pattern using Clewin or AutoCAD and then writing the pattern on a chrome-plated soda glass plate that serves as our master mask by the mask maker. With the mask we made, we are able to get good patterned substrates by using the SUSS Mask Aligner MJB4 in the clean room. We also successfully deposited several kinds of metals, such as Au/Ti and Cr, on the substrates using an e-beam evaporator and sputtering system. Moreover, we successfully etched the substrate by reactive ion etching (RIE) with a Cr pattern intact to fabricate trenches on the substrate. RIE is favored over wet-etching as it is an anisotropic etching process, leading to a better side-wall profile. The above-mentioned process has been optimized to obtain preliminary trench pattern on quartz substrates.

As the first application of our developed photolithography procedure, we made a quartz substrate with pattered electrodes, shown in Fig. 3. With this sample we performed the first low-temperature micro-PL experiments on individual SWNTs in the presence of external electric fields, as described below:

Module 2. Low Temperature μ-PL Spectroscopy of SWNTs in Electric Fields:

To observe FES in nanotubes, it is essential to study them on a single-tube level. This can be made possible by performing micro-PL spectroscopy at low temperatures. A low-temperature environment is important to assure that the system is degenerate.

The SWNTs used in our experiments were HiPco carbon nanotubes dispersed in surfactants such as SDBS and sodium cholate. The average length of the SWNTs in the sample was less than 1 μm. The sample was prepared by further diluting (10:1) the parent nanotube solution using the same surfactant solution and spreading a few drops of this diluted solution evenly on 350 μm, double-side polished, crystalline quartz substrates (~15 mm x 15 mm). The excess nanotube solution was blow-dried with nitrogen to obtain an areal density of about 1 nanotube per μm^2. The choice of crystalline quartz for the substrate was made, given its high transparency and negligible PL of its own.

In order to apply an electric field on the nanotubes, we made a quartz substrate with specially designed electrodes. Figure 3 (top) shows a side view of the sample we made. The

Au/Ti/Cr contacts were made on the quartz substrate by photolithography and deposition through sputtering, and subsequently lifting off the metal. On this substrate, we deposited HiPco carbon nanotubes using the same procedure as the last paragraph. Then, we made wire connection between the contacts and the electrical pads in the cryostat so as to apply an electric field. The electric field strength is given by $E = V/d$, where d is the distance between two contacts we made (between 5 μm and 50 μm in our experiments), and V is the applied voltage.

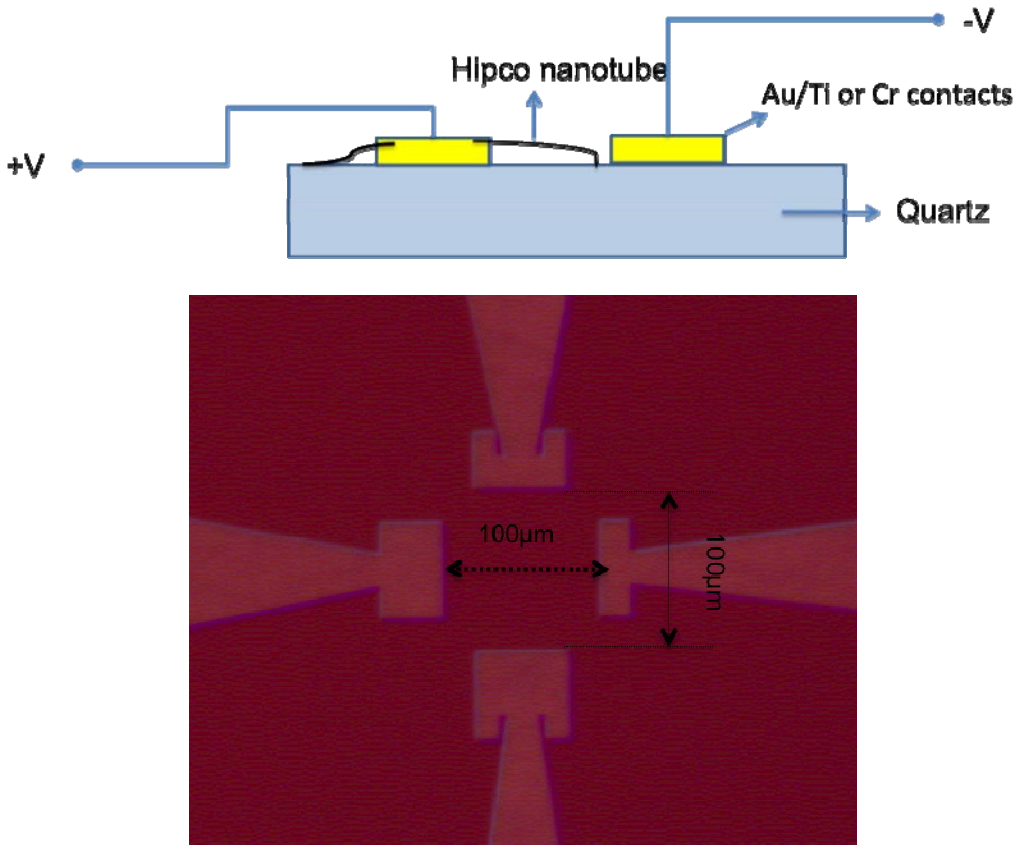

Figure 3. Schematic diagram (top) and picture (bottom) of the sample used in the micro-PL experiments in the presence of electric fields.

Figure 4 shows a schematic of our experimental setup. A tunable Ti:Sapphire laser is used as the excitation source with a tuning range of 760 nm - 850 nm. It is operated in continuous-wave (CW) mode with an output power of up to 500 mW at 800 nm. After going through appropriate filters, the laser beam is focused onto the sample, and the PL is collected by the objective lens on the other side of the sample. The focal size of the laser beam at the sample is ~60 μm. The objective lens used is an infinity-corrected 40X near-infrared Mitsutoyo objective with a working distance of 17 mm and a numerical aperture (N.A.) of 0.42. This long working distance is required to image the sample which is mounted inside of a liquid helium flow cryostat. The cryostat is specially designed for microscopy applications with low thermal drift and vibration and can cool down the sample to liquid helium temperatures. The cryostat itself is mounted on a 2-axis motorized stage with 100 nm resolution to position the required sample area in the field of view of the objective lens. The PL from the sample is emitted in all directions, while only the part of PL which is within the N.A. of the objective lens is collected.

The PL is then imaged onto the entrance slit of a 300-mm focal length spectrometer using a 200-mm focal length plano-convex lens. In order to block any reflected laser light from entering the spectrometer, appropriate long-pass filters are used. A 300g/mm grating blazed at 1 μm is used to disperse the PL spectra before it is detected by a liquid-nitrogen-cooled 2D InGaAs focal plane array (FPA) with 320 x 256 pixels. This detector is sensitive to light in the range of 900 nm - 1600 nm. In order to perform polarization-dependent studies, half-wave plates, quarter-wave plates, and polarizers are used to control the polarization of the laser and the emission independently.

Figure 4. A schematic diagram of the micro-PL experimental setup.

This setup is versatile enough to use other laser sources such as laser diodes, Nd:YAG lasers, and other detectors such as Si CCD to cover a vast spectral range in both excitation and emission. Moreover, it can also be used to study μ-Raman spectra of SWNTs using appropriate filters. The magnification of the setup was characterized by illuminating a USAF resolution target with known pattern dimensions, using a fiber lamp and a 1/3" Si CCD. Next, the spot size of the laser was measured relative to the known calibration.

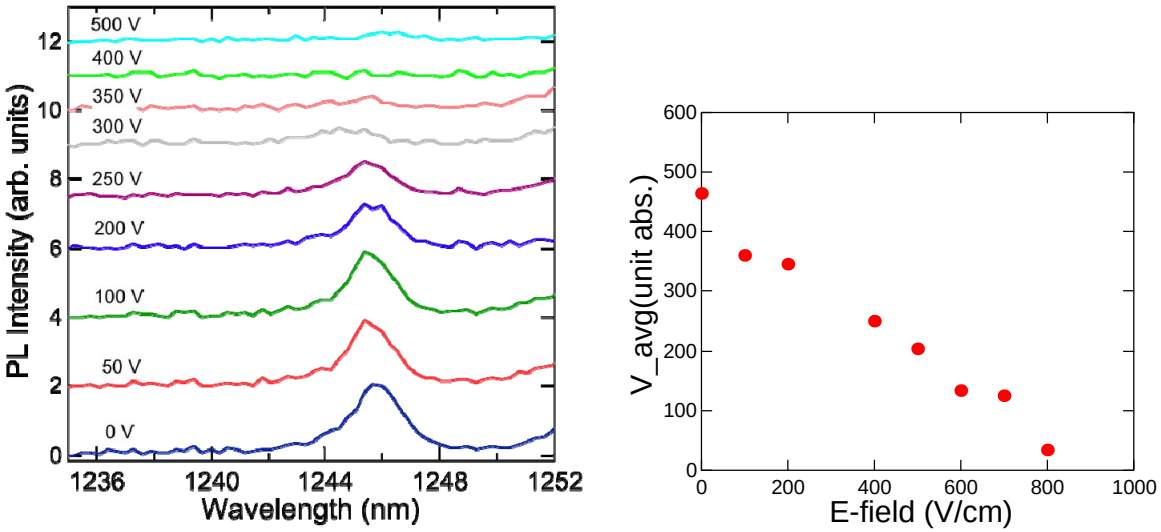

Figure 5. Electric-field-dependent photoluminescence spectra of a single single-walled carbon nanotube, showing an unusual "quenching" of PL intensity when a parallel *E*-field is applied.

Using this setup we obtained some data under an electric field, as shown in Fig. 5. From the result we can see a "quenching" of PL intensity when a parallel electric field is applied. Further experiments are underway to understand this novel effect.

Module 3. Low Temperature μ-PL Spectroscopy of SWNTs in Magnetic Fields:

Valley Degeneracy and "Dark" Excitons

SWNTs are unique due to their special chirality-dependent symmetry that also manifests itself in the band structure. In particular, there are two energy bands, or valleys, that are related to each other through time-reversal symmetry. In determining the optical selection rules, one also needs to take into account how the "symmetry" of the perturbation (electromagnetic in this case) couples two eigenstates of different symmetries in finding which optical transitions are allowed ("bright") and which are forbidden ("dark"). These facts lead to a rich excitonic fine structure in SWNTs, which remain to be explored experimentally. Recall that out of the 16 excitonic states possible for the lowest quasi-angular momentum index $i = 1$ or the E_{11} excitonic manifold, 12 spin-triplet states are optically inactive, or dark, in the absence of spin-flip scattering. Even amongst the four remaining spin-singlet states, the two indirect excitons are optically forbidden due to the conservation of linear momentum unless some other elementary excitation, say, a phonon provides the required momentum. Through parity considerations of the remaining two direct excitons, it is shown that only one is optically allowed and lies above the lowest energy spin-singlet dark exciton. Experimentally, the excitonic fine structure is not very well understood, and even the theoretical predictions about the various excitonic states and their relative energies with respect to each other still remain controversial. Although it is widely believed that this dark state lies lower than the bright state irrespective of the chirality of the semiconducting nanotube, there is no consensus as to the value of spin-singlet dark-bright splitting, theoretical predictions ranging from a few to hundreds of meV. A detailed study of the excitonic fine structure of SWNTs is thus essential for resolving these discrepancies and

furthering our understanding of radiative and non-radiative energy relaxation processes in SWNTs. From an applications point of view, the existence of dark excitons has often been evoked to explain the observed low quantum efficiency of SWNTs. Any useful optoelectronic application is possible only after a detailed study of various dark excitons and how they behave under the influence of symmetry breaking perturbations.

Previous experiments done on ensembles of nanotubes have provided some evidence for "magnetic-brightening." In particular, in the presence of high magnetic fields up to 70 T, the PL intensity was seen to increase at low temperatures. Due to the broad linewidths of PL in such experiments, however, any direct measurement of the dark-bright splitting was impossible, and its value was inferred indirectly from data-fitting. Moreover, only a *mean* value of this splitting could at best be estimated from the data due to the fact that the whole ensemble was probed at the same time. The most direct way to "observe" the dark excitons in SWNTs is to perform spectroscopy on single nanotubes at low temperature such that the linewidths are smaller than the dark-bright splitting Δ_x and then apply a magnetic field to brighten the dark excitons. Such methods have been used to prove the existence of dark excitons in semiconductor quantum dots. To probe the intrinsic fluctuations that are dominant at nanoscale, local probing, as opposed to ensemble averaging of their properties, is essential for revealing the individuality of nano-sized materials. Spectroscopy on a single nanotube can also give us insight into the role of the local environment surrounding the nanotube, which can cause significant changes in emission energies and radiative lifetimes.

Here, we discuss our low-temperature μ-PL experiments done on *individual* SWNTs under magnetic fields, which have led us to unambiguously "observe" the dark exciton for the first time in SWNTs. We have relied on symmetry breaking and the Aharonov-Bohm effect to "brighten" the dark exciton state, and thus observe it optically in the PL spectra. In addition, we have, for the first time, identified the relative energies of the bright and dark excitons and found them to be much smaller than many theoretical predictions. This dark-bright splitting was found to be different for different tubes within the same chirality, hinting at the role of local environment in determining the excitonic fine structure.

Experimental Results and Discussion

Figure 6 shows typical *B*-dependent single-tube PL spectra taken at $T = 5$ K. At $B = 0$, a single, sharp peak exists. As B is increased, a second peak appears at a lower energy than the first peak. With further increase of B, it sensitively increases in intensity with increasing B, at the expense of the bright exciton peak, and quickly becomes the dominant PL feature at $B > 3$ T. The splitting between the two peaks also increases with B. This B-induced appearance of a lower energy peak was universally observed in all of the 50+ nanotubes of different chiralities which were *not* completely perpendicular to B.

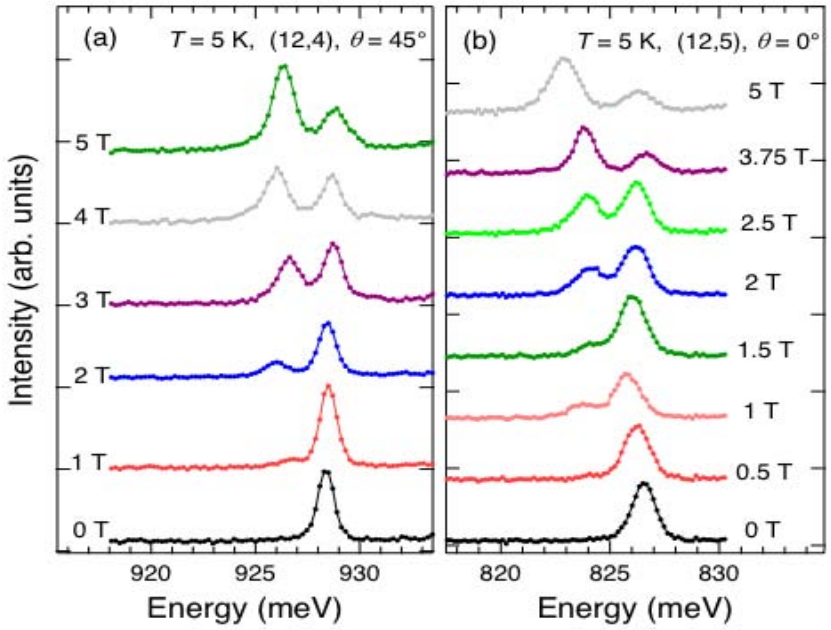

Figure 6. Typical magnetic-field-dependent PL spectra for a single (12,4) tube (a) and a single (12,5) tube (b), showing the appearance of a "dark exciton" peak at a lower energy with respect to the main bright emission peak when a magnetic field is applied parallel to the tube axis. The peak grows with the field at the expense of the bright emission peak and becomes dominant at fields > 3 T.

In Fig. 7, typical PL spectra for SWNTs oriented *completely perpendicular* to B are shown. Clearly, there is no appearance of any lower energy peak even at the highest fields. We emphasize that we did not observe two PL peaks for any nanotube that was completely perpendicular to the field. Even in the parallel configuration, only the tubes which had $\theta < 65°$ showed any observable magnetic brightening of the dark state. Assuming a completely random distribution of θ, this corresponds to ~72% of all the tubes. Indeed, out of the 75 nanotubes studied in the parallel configuration, 55 tubes (73%) showed magnetic brightening as is expected from a random distribution of θ. This also implies that all tubes in our sample emit from the higher energy state at zero field.

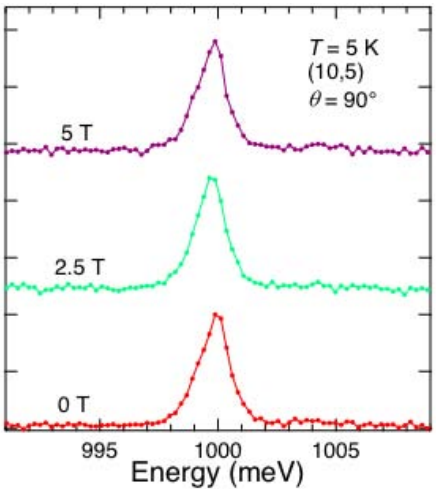

Figure 7. Typical magnetic field dependence for the case of a perpendicular magnetic field. Clearly, no magnetic brightening of the dark exciton peak is seen.

To quantitatively explain our observations, we use a two-level model described in our earlier reports [Shaver *et al.*, *Nano Letters* **7**, 1851, (2007); Shaver *et al.*, *Physical Review B* **78**, 081402(R) (2008)]. We assume that at zero field the dark state is completely dark while the bright state has a relative oscillator strength of 1. The total dark-bright splitting Δ in the presence of tube-threading magnetic flux Φ is given by

$$\Delta^2 = \Delta_x^2 + \Delta_{AB}^2, \qquad (1)$$

where Δ_x is the zero-field splitting, $\Delta_{AB} = \mu\Phi + \Delta_{dis}$, μ is a coupling constant, $\Phi = \pi d^2 B_{\|}/4$, d is the tube diameter, $B_{\|} = B\cos\theta$, and Δ_{dis} is the disorder-induced zero-field splitting. In the following, we do not include Δ_{dis}, whose existence would imply zero-field brightening of the dark state. Indeed, we only see a single emission peak from the bright state when $B_{\|}$ = 0 for any tube, suggesting that the effect of disorder in brightening the dark state is negligible in our sample. We use Eq. (1) to fit the splitting value versus $B_{\|}$, obtained directly from the PL spectra at different fields. The offset and slope of the linear fit between Δ^2 and $B_{\|}^2$ give us Δ_x and μ, respectively, as shown in Fig. 8. The possible experimental uncertainty in the value of Δ_x thus obtained arises from the finite bandwidth/pixel of our spectroscopy system and is estimated to be less than 12%. The error in the fit is found to be smaller than the instrument-limited error.

Figure 9(a) shows Δ_x for 45 different tubes versus tube diameter and emission wavelength (inset). The value of Δ_x is less than 4 meV for the majority of the tubes. These values (1-4 meV) agree well with those of our prevuous measurements on ensemble samples but should be contrasted to the large (10-100 meV) values predicted by some theoretical studies. A possible cause of this discrepancy could be the difference in the value of the dielectric constant (ε) used in the calculations. An accurate prediction must not only take into account the dynamically-screened potential arising from the many-body interactions within the nanotube but also the local variations in ε due to the medium surrounding it (e.g., surfactant, water, quartz substrate). The dielectric confinement arising from the difference in ε between the nanotube and the surrounding medium causes image charges that can modify both the exciton binding energy and Δ_x.

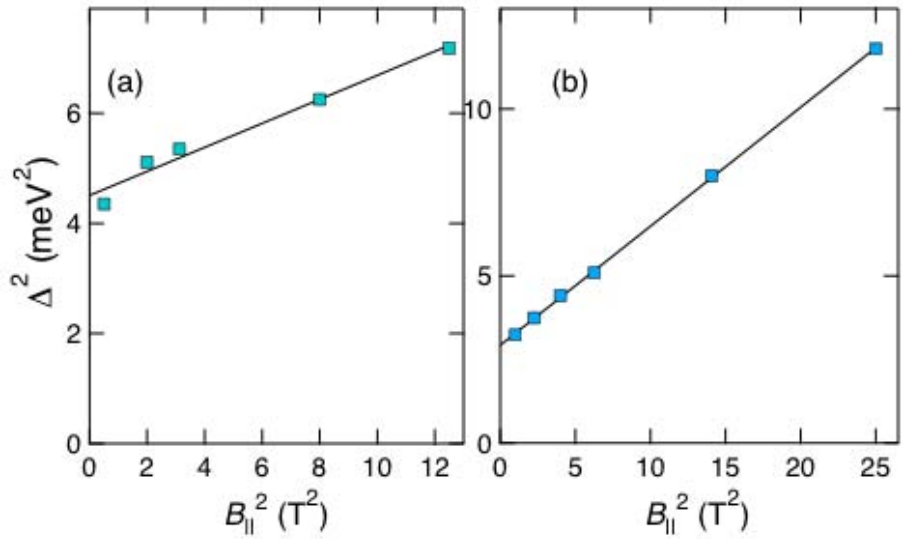

Figure 8. Linear fit of the data in Fig. 6 using Eq. (1), to obtain Δ_x from the offset and μ from the slope.

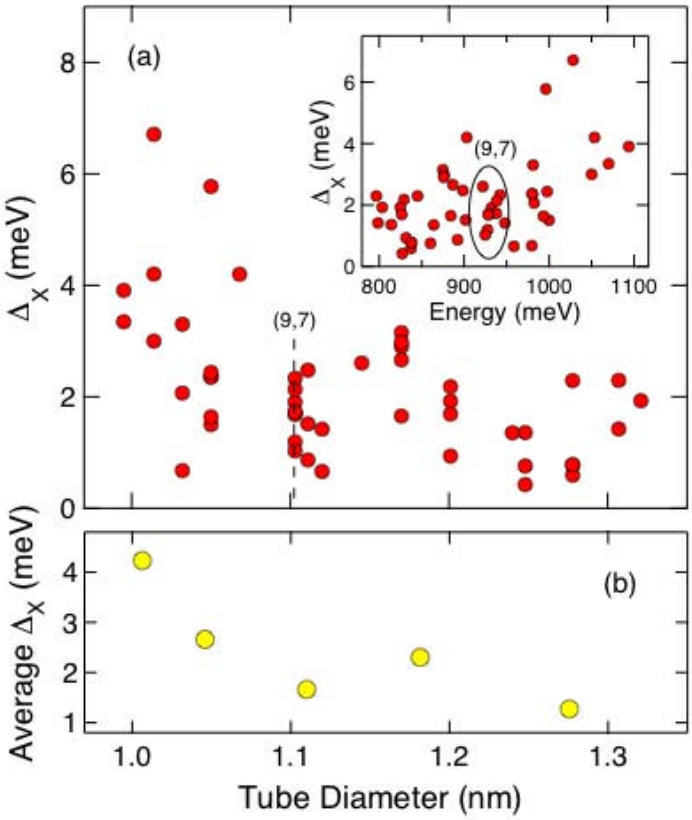

Figure 9. (a) Measured zero-field dark-bright splitting, Δ_x, as a function of tube diameter for 45 tubes. The data shows scatter even for tubes with the same chirality. Inset shows the same data plotted against emission wavelength before the assignment of respective chiralities. Structural assignment was done based on room temperature photoluminescence excitation spectroscopy data taking inhomogeneity of emission wavelength into account, as shown representatively for (9,7) species. (b) The data in (a) is averaged over 5 diameter ranges and plotted against average diameter to highlight the trend of decreasing Δ_x with increasing diameter.

Another striking observation one makes from Fig. 9(a) is that the value of Δ_x shows scatter even for tubes of the same chirality. This scatter is most likely to arise from the fluctuations in the local environment of the tubes. Micro-PL spectroscopy is a powerful probe for such fluctuations and enables us to study the role played by the local environment in determining the excitonic fine structure. Since Δ_x is determined by the exchange interaction, it can vary from tube to tube if the local ε varies. Thus, such local variations of ε can lead to "inhomogeneous broadening" of Δ_x. For example, according to a recent theoretical estimate, a change of $\varepsilon = 3$ to $\varepsilon = 2$ leads to a change in Δ_x from ~6 meV to ~2 meV for an (11,7) nanotube. To extract any trend that is present in the d dependence of Δ_x, we averaged Δ_x over five d ranges. This average Δ_x, plotted in Fig. 9(b), decreases with d, which is reasonable because the short-range Coulomb interaction is predicted to decrease with d. However, an exact functional form of the d dependence is difficult to deduce from Fig. 9(b) due to the insufficient number of data points. From Eq. (1) and Fig. 10 we obtain values of μ of 0.4-1.0 meV/T-nm^2 for most nanotubes. These values agree well with the theoretical predictions as well as previous measurements on ensemble SWNT samples in high magnetic fields. A possible error in

determining the value of μ arises from the uncertainty in determining θ. We estimate this uncertainty to be ~2° (or 35 mrads). This error in θ translates to an error in μ of less than 0.025 meV/T-nm^2 for nanotubes with $\theta < 30°$ but increases rapidly to 0.12 meV/T-nm^2 for tubes with $\theta = 60°$.

Finally, we analyze how the relative intensities of the two peaks change as a function of *B*. Even though the absolute intensity of each peak was subject to blinking, the relative intensities were not affected by any intensity fluctuations. Within our two-level model, the intensity ratio of the two peaks is given by

$$\frac{I_\delta(B_\parallel)}{I_\beta(B_\parallel)} = \exp(\frac{\Delta}{k_B T}) \frac{f_\delta(B_\parallel)}{f_\beta(B_\parallel)}, \qquad (2)$$

where k_B is the Boltzmann constant and $f_{\delta,\beta}(B_\parallel)$ are the oscillator strengths of the dark (δ) and bright (β) levels in the presence of $B_\parallel$, which vary as

$$\frac{f_\delta(B_\parallel)}{f_\beta(B_\parallel)} = \frac{1-\frac{\Delta_x}{\Delta}}{1+\frac{\Delta_x}{\Delta}}. \qquad (3)$$

Equation (2) allows us to extract the oscillator strength ratio f_δ / f_β from the experimentally-measured intensity ratio (I_δ / I_β) and splitting (Δ) for each $B_\parallel$. This quantity, when plotted versus Δ_x / Δ, should exhibit the same functional form given by Eq. (3) for *all* nanotubes. Figure 10 shows the oscillator strength ratio as a function Δ_x / Δ of for 9 different nanotubes of varying chiralities. We find that the data points for all nanotubes indeed follow the universal curve given by the right-hand side of Eq. (3), in remarkable agreement with the theory. The *T* used to evaluate the Boltzmann factor was obtained from fitting the ratio of intensities at different values of $B_\parallel$ for a particular nanotube according to Eq. (2) as shown in the inset of Fig. 10. This value of *T* was then used for all the nanotubes plotted in Fig. 10. The obtained value of T_{fit} = 10 K was slightly higher than the temperature read from the sensor T_{sensor} = 5 K placed more than 10 mm away from the sample. This difference could easily arise from the thermal gradient between the locations of the temperature sensor and the sample.

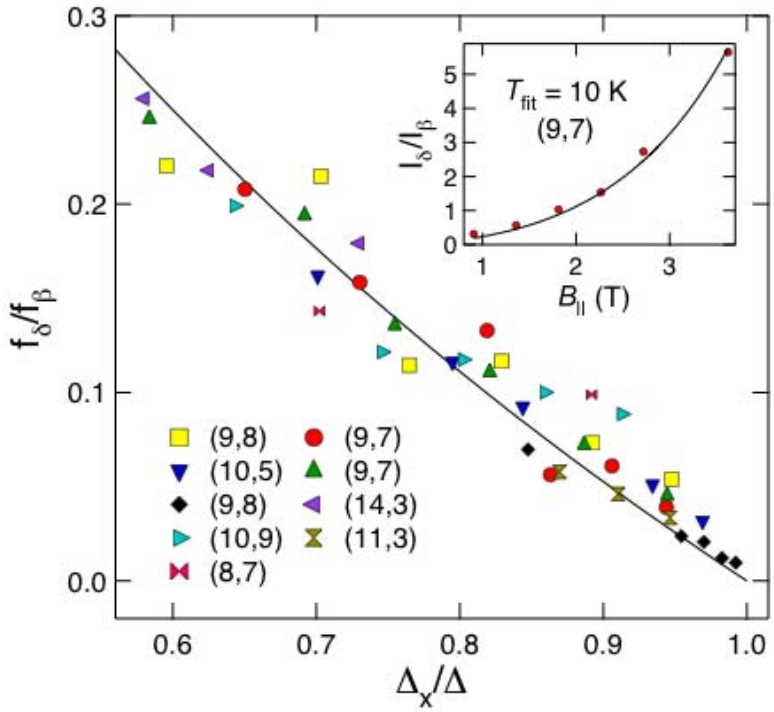

Figure 10. Dark (δ) / bright (β) oscillator-strength ratio for 9 different nanotubes versus zero-field dark-bright splitting (Δ_x) normalized to the finite-field splitting (Δ). They all fall onto a single curve given by Eq. (3). The temperature of all nanotubes was taken to be 10 K, which was obtained by fitting the intensity ratio against $B_{||}$ to Eqs. (2) and (3), as shown in the inset. This value is very close to the measured temperature of 5-7 K.

In conclusion, we have unambiguously demonstrated the existence of the theoretically-predicted spin-singlet dark exciton state below the bright state. The dark-bright splitting was directly measured and found to be 1–4 meV for tubes with diameters of 1.0–1.3 nm. Scatter in splitting value suggests the importance of the local environment in determining the excitonic fine structure.

For more details, see A. Srivastava, H. Htoon, V. I. Klimov, and J. Kono, "Direct Observation of Dark Excitons in Individual Carbon Nanotubes: Inhomogeneity in the Exchange Splitting," *Physical Review Letters* **101**, 087402 (2008).

Project 2: Electron Spin Resonance of Carbon Nanotubes

Introduction:

In one-dimensional (1-D) systems, electronic correlations are too strong to be screened, leading to the breakdown of Fermi-liquid theory. Fortunately, however, 1-D electronic systems are theoretically well understood as Tomonaga-Luttinger Liquids (TLLs), wherein Fermionic quasi-particles no longer exist, being replaced by collective, or bosonic, excitations. One of the most striking predictions of TLL theory is *spin-charge separation*. This theoretical result flows from the idea that in a TLL, the collective spin ('spinon') and collective charge ('holon') are separate entities. Essentially, when an interaction, such as a magnetic or electric field, is applied to a 1-D metal, the spinon and holon couple differently to this interaction. This symmetry breaking is expected to manifest itself in the form of two different resonances that diverge with increasing applied field.

Single-walled carbon nanotubes (SWNTs) are ideal environments for exploring TLLs, since their high aspect ratio of length to diameter (~10000:1) allows us to treat them as one-dimensional structures. Furthermore, SWNTs can either be semiconductors or metals, giving us at least two ways to explore TLLs: doping of the semiconducting SWNTs or separating out the metallic ones. Both approaches are feasible and are actively being pursued by several groups in the field, including ours.

To actually explore spin-charge separation in SWNTs, we proposed using electron spin resonance (ESR) at high magnetic fields. ESR in metals has the ability to measure four things: first, it probes the spin population, which is proportional to the spin susceptibility of the sample; second, the spin-orbit environment can be examined through the shift of the g-factor from the free electron value ($g = 2.0023$); third, the spin-spin dephasing time, or spin relaxation time (T_2), is found by looking at the width of the resonance; and fourth, the shape of the resonance peak gives an idea of the type of environment the electrons are in (i.e., localized, inhomogeneously broadened, diffusive, etc.). As stated before, the different coupling of the spinon and holon to interactions (in this case, a magnetic field) can result in diverging behaviors. Drawing from theoretical research, we are predicting that the ESR resonance peak in SWNTs will begin to split at high magnetic fields and low temperatures as the spinon and holon energies differ by an amount proportional to the magnetic field.

The first step to understanding ESR in nanotubes is to study the bulk response. Over the past two decades, a variety of publications have reported on ESR in nanotubes. Conflicting results and interpretations suggest that much work in this area still needs to be done. In particular, the magnitude and temperature dependence of the spin susceptibility, χ, and the ESR lineshape have both seen widely diverging results in the literature. Moreover, sample conditions, such as the presence of adsorbed molecules, SWNT compaction density, and nanotube alignment, have not been controlled in previous studies. In what follows, we present a systematic temperature study of spin resonance in an ensemble of nanotubes with and without oxygen, a molecule which we found to strongly affect spin dynamics in SWNTs. Our results suggest that the movement and interactions of the electron spins in nanotubes are influenced by the presence of oxygen. Strikingly, cross-over from a 3-D to a 1-D description of the SWNT

bulk may be caused by removing oxygen, suggesting that oxygen may play the same role in nanotubes as it does in 1-D polymers, such as polyaniline.

Achievements During the Last 12 Months:

The last year has seen two major advances for this project. First, we created a methodology for producing samples that were condensed, fixed SWNT plates, which allowed us to perform highly repeatable and systematic ESR measurements. Second, we discovered that removing oxygen substantially enhances the spin susceptibility of nanotubes. In Module 1, we present data from the same SWNT pellet in two conditions: (1) water-free and (2) both water- and oxygen-free. Since only the concentration of oxygen is different between the two samples and no water exists in either condition, this systematic temperature study yields deep insight into the role oxygen plays in the electron spin dynamics in nanotubes.

In Module 2, we present our progress on single-tube ESR measurements. Two different processes are currently under development to create a single-tube field-effect transistor (FET). By using the CNT-FET in combination with a Helium 3 dilution refrigerator in a high magnetic field (10 T), we hope to detect ESR in a nanotube this year.

Module 1: Temperature Dependent ESR Measurements of Oxygen-free Single-Walled Carbon Nanotubes

Accomplishments:

A method for producing condensed, immobile plates of nanotubes was developed so that reproducible ESR measurements could be made. In previous measurements, movement of macroscopic nanotube granules altered how much microwave energy was absorbed, since tube-tube contact (and thus conductivity) was changed. Producing a nanotube 'plate,' we were able to avoid problems related to movement and reproducibility. Correct sample formation allowed us to perform temperature-dependent ESR measurements on a sample in two different conditions: water-free and both water- and oxygen-free. Both sample states showed linewidth motional narrowing, a phenomenon never observed before in nanotubes. Also, a large increase in the spin susceptibility occurred when oxygen was removed. Strikingly, not only did the magnitude of the spin susceptibility change, but also its temperature dependence, going from a Curie-law ($1/T$ behavior) to a non-Curie-law trend.

At selected temperatures, power saturation spectroscopy was performed to obtain information regarding population decay times (T_1) and dispersion to absorption ratios (α). We observed both signal saturation of the absorption signal and a change in α at high microwave power. Further investigation is needed to understand this absorption saturation behavior.

Details:

Methods

The sample used in the ESR experiments was composed of acid purified laser oven nanotubes from NASA. The acid purification process reduces the ferromagnetic catalyst concentration to ~5.5% by mass as measured by x-ray photoelectron spectroscopy (XPS) and thermal gravimetric analysis (TGA). Water was then added to the dry nanotube powder. Next, we sonicated the mixture for two hours in a bath sonicator to break up the large and uneven nanotube macroscopic granules. This step was followed by a four-hour ultracentrifugation to create a compacted, dense, and relatively homogeneous flat mass of SWNTs.

We removed all the remaining water from the ultracentrifugated nanotube film by placing it into a dessicator for ten days. The resulting sample condition, which we term 'water-free,' was then measured by an ESR spectrometer at numerous temperatures from 3.7 K to 300 K. Next, the same sample was placed into an argon furnace at 115 °C for 24 hours to remove oxygen from the nanotubes; we refer to this sample condition as 'oxygen-free.' As with the water-free sample condition, temperature-dependent ESR measurements were made from 3.4 K to 300 K. For both sample conditions, power saturation spectroscopy was performed at selected temperatures. A power scan consisted of changing the incident microwave power from 6 μW to 200 mW in 3 dB (factor of two) steps.

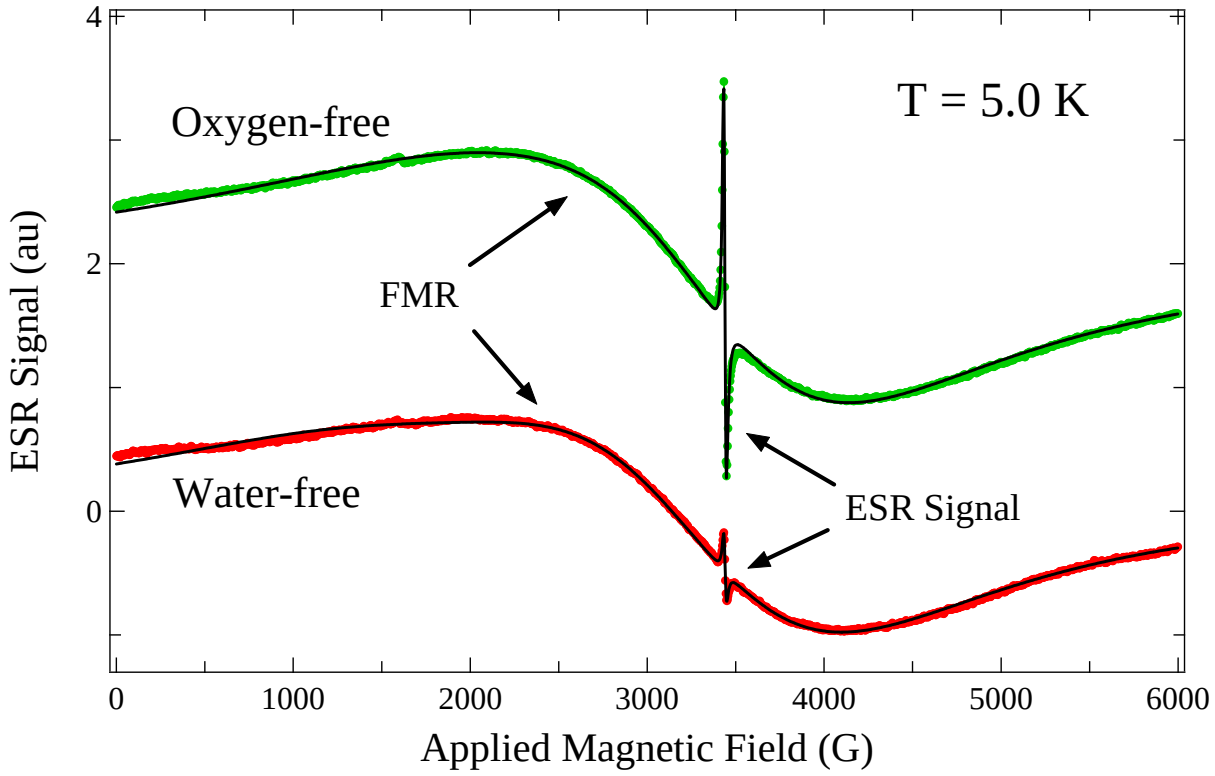

Figure 1. Scans at 5.0 K for both the water-free and oxygen-free sample conditions from 0 to 6000 G. Both the ferromagnetic resonance (FMR) due to remaining catalyst particles and the ESR signal from SWNTs can be fit very well using a Dysonian curve for the ESR signal and two Lorentzians for the FMR curve. Note that ESR signal is actually larger than the FMR signal in the oxygen-free state. The traces are intentionally offset for clarity.

As Fig. 1 shows, a ferromagnetic resonance (FMR) from catalyst particles in the nanotubes creates a very large background on which the main ESR nanotube signal sits. Long scans, such as those seen in Fig. 1, can be fully fit using a Dysonian curve (main nanotube resonance) and two Lorentzian curves (FMR background). We believe that the two Lorentzian resonances describe the presence of cobalt and nickel catalyst particles; this hypothesis agrees with previous ESR nanotube studies. The three curve fitting scheme also produces excellent fits for the short, detailed scans of the ESR resonance (see Fig. 2). It is from these short scans of the resonance that we extract the data that will be presented later. As a note, the long scan results that we have obtained are the only known instance in which the ESR resonance is larger than the FMR background resonance; we observe this behavior at low temperatures (T < 10 K).

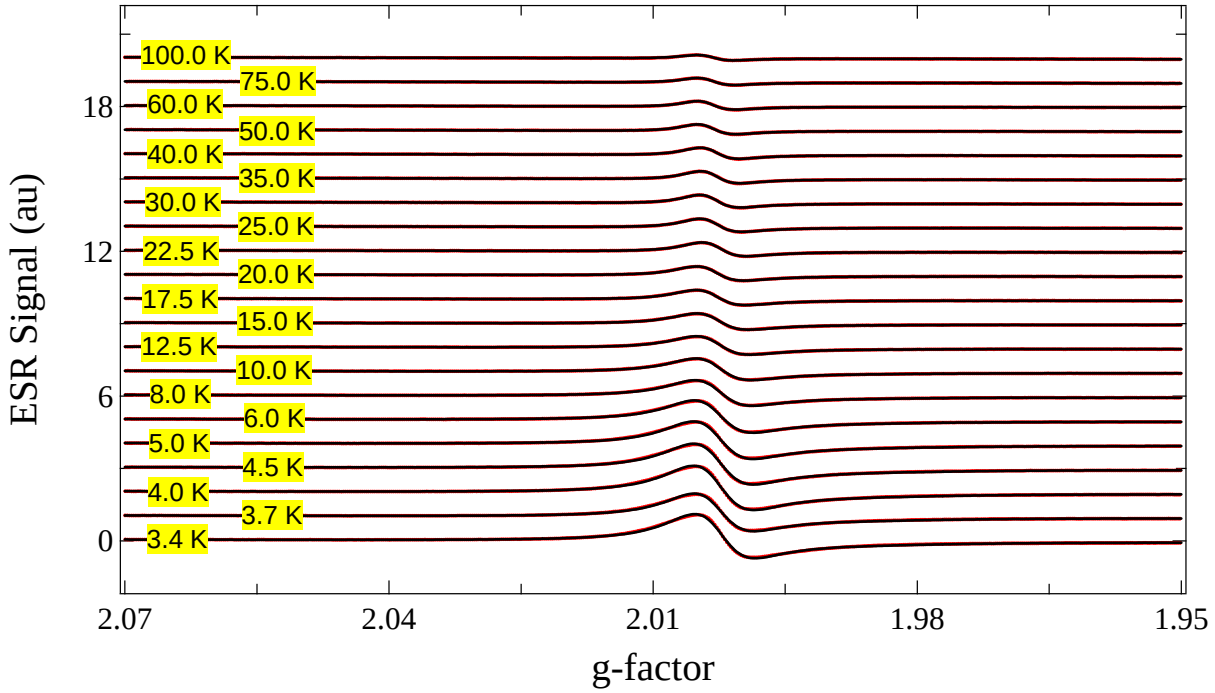

Figure 2. Raw ESR data with curve fits for the oxygen-free condition from 3.4 K to 100 K. The spectra are intentionally offset for clarity.

Dysonian Lineshape

Since the conductivity of nanotubes is higher than an insulator but lower than a true metal, we expect that some curve asymmetry will be present in the ESR spectrum. Conceptually, when mobile (conduction) electrons are able to randomly move in and out of the coherent microwave field, the resulting ESR lineshape will have dispersion; often, this lineshape can be theoretically described using a Dysonian curve [G. Feher and A. F. Kip *Physical Review* **98**, 337 (1955) and F. J. Dyson *Physical Review* **98**, 349 (1955)]. For the case of a weakly conductive medium, such as nanotubes, the Dysonian lineshape can be approximated by an admixture of a Lorentzian curve and a dispersion curve

$$\frac{dP}{dH} = A\frac{d}{dH}\left(\frac{\Delta H}{\Delta H^2 + (H - H_0)^2} + \frac{\alpha(H - H_0)}{\Delta H^2 + (H - H_0)^2}\right),$$

where A is related to the number of spins probed, ΔH is the linewidth, H_0 is the center of the resonance, and α measures the ratio of the dispersion to the absorption. Instead of H_0, we often look at the g-factor as a measure of the center of the resonance, where $g = \frac{h\nu}{\mu_B H_0}$, μ_B is the Bohr magneton, and ν is the microwave frequency. Furthermore, in this formulism, A is proportional to the spin susceptibility, χ, which relates the magnetization of a given medium (M) to the applied magnetic field (H) via

$$M = \chi H .$$

By analyzing χ, the g-factor, ΔH, and α as a function of temperature, we can obtain a profound insight into spin dynamics. In particular, the temperature profile of χ can give information about quantum mechanical processes if deviations from Curie-law behavior are observed.

Experimental Results and Discussion

Figure 2 shows the results of the curve fitting for the oxygen-free data from 3.4 K to 100 K. The curves fit exceptionally well to experimental data with the ESR nanotube resonance being given by the weak Dysonian form previously described. Three qualitative observations should be pointed out. First, the signal intensity (a statement of spin susceptibility) grows as the temperature decreases. This behavior, which is also seen in the water-free data, conflicts with previously published results, which saw the signal intensity rise until 15 K before precipitously dropping from 15 K to 4 K [V. Likodimos *et al.*, *Physical Review B* **76**, 075420 (2007)].

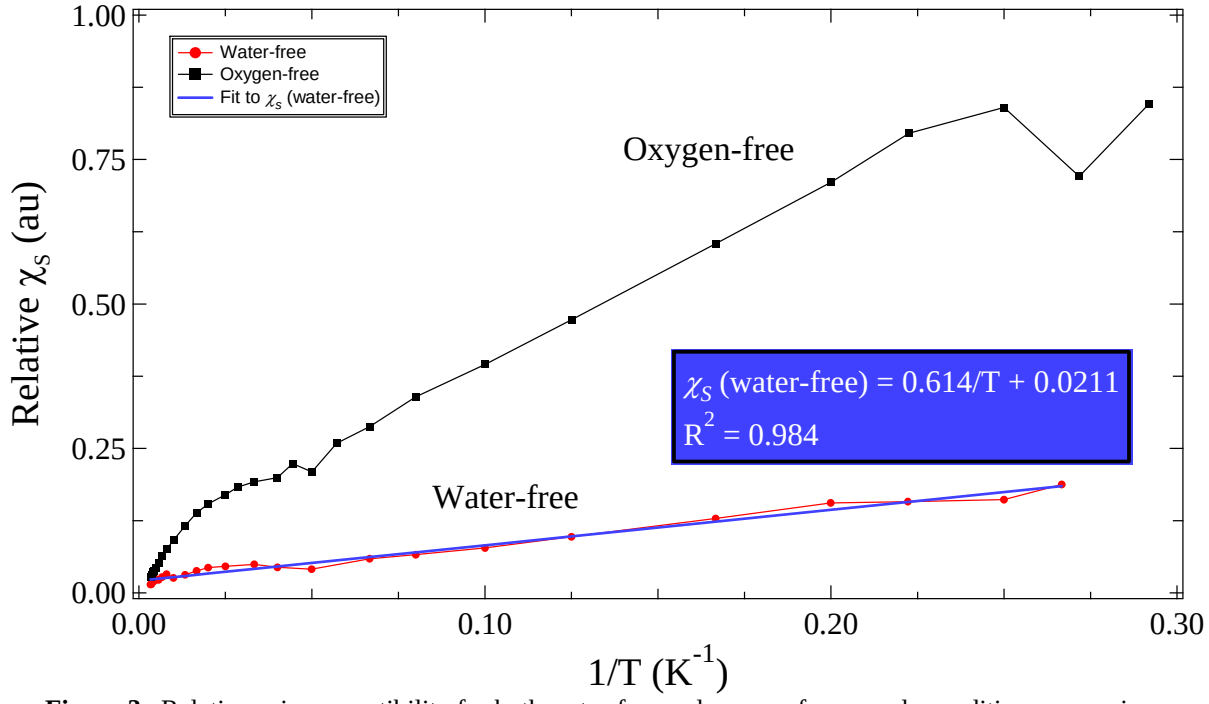

Figure 3. Relative spin susceptibility for both water-free and oxygen-free sample conditions versus inverse temperature. A Curie-law trend with a Pauli constant describes the water-free data very well. The oxygen-free spin susceptibility is roughly four times as large as the water-free data. In addition, the oxygen-free spin susceptibility does not display a typical Curie-law behavior, despite a clear rise in value with decreasing temperature.

Second, the linewidth increases with decreasing temperature. This important observation indicates that the spin relaxation dynamics are changing as a function of temperature. Prior work, e.g., Likodimos *et al.*, showed the linewidth to be constant as a function of temperature. Last, the *g*-factor is relatively temperature independent and is very close to the free electron value of 2.0023. This behavior is expected and has been observed before by many other researchers.

In Fig. 3, relative spin susceptibility, $\chi_{s,}$ is plotted versus $1/T$. As can be seen from the figure, the water-free spin susceptibility follows a Curie-law ($1/T$) behavior with a Pauli law (temperature independent) contribution, $\chi_{0,}$

$$\chi_S = \frac{C}{T} + \chi_0 .$$

Employing this equation to fit the water-free data, we find that the Curie constant, C, is roughly one order of magnitude larger than χ_0. The fact that C is much larger than χ_0 and that χ_s follows a $1/T$ trend implies that the ESR signal is due mostly to fixed spins. Yet, as the presence of dispersion in the ESR lineshape shows, there is a non-negligible contribution from mobile spins. The water-free spin susceptibility data represents the first observation of Curie-law behavior in nanotubes (Likodimos *et al.* saw Curie-law behavior from 300 K to 15 K, but not for lower temperatures).

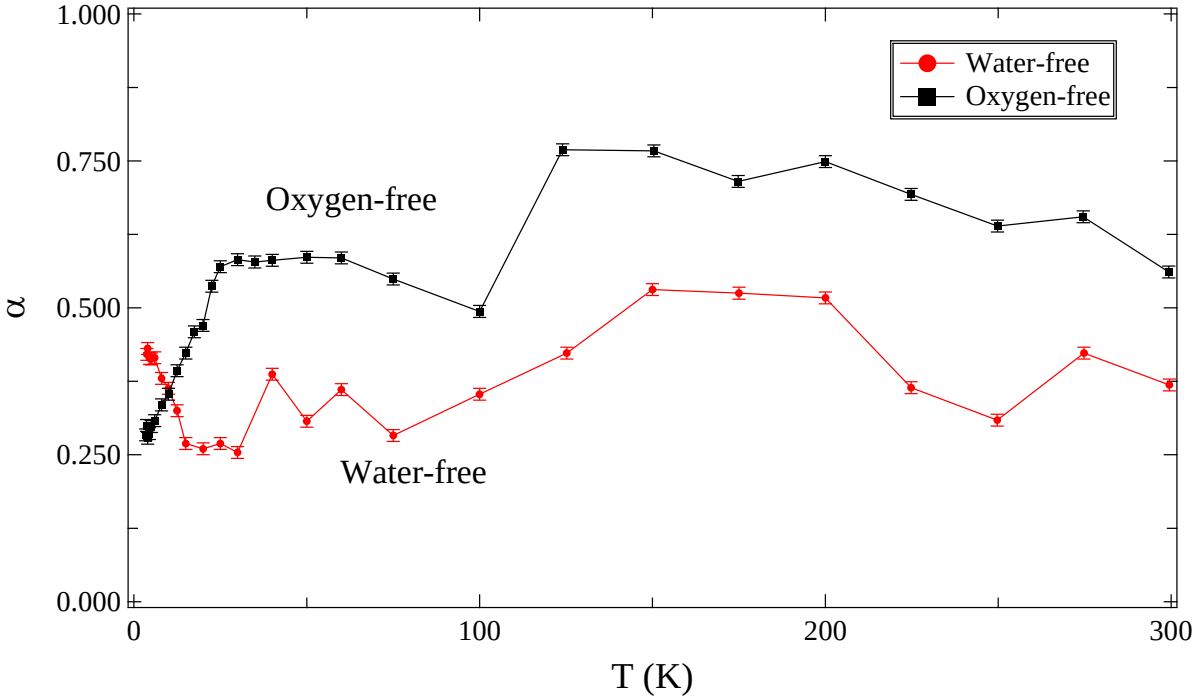

Fig. 4. Dysonian asymmetry factor, α, as a function of temperature for both the water-free and oxygen-free sample conditions. The oxygen-free α value increases as temperature is increased, indicating increased spin movement.

The oxygen-free χ_s data paints a different picture than the water-free condition. First, the oxygen-free spin susceptibility magnitude is roughly four times larger than the water-free χ_s values, suggesting that oxygen has a strong effect on the coherent excitation of spins in nanotubes. Strikingly, when oxygen is removed, χ_s no longer follows a $1/T$ behavior; this may

point to interesting physics related to strong quantum confinement. We estimate that the magnitude of the oxygen-free χ_s data is largest ever observed in nanotubes, although further calculations are necessary to confirm this.

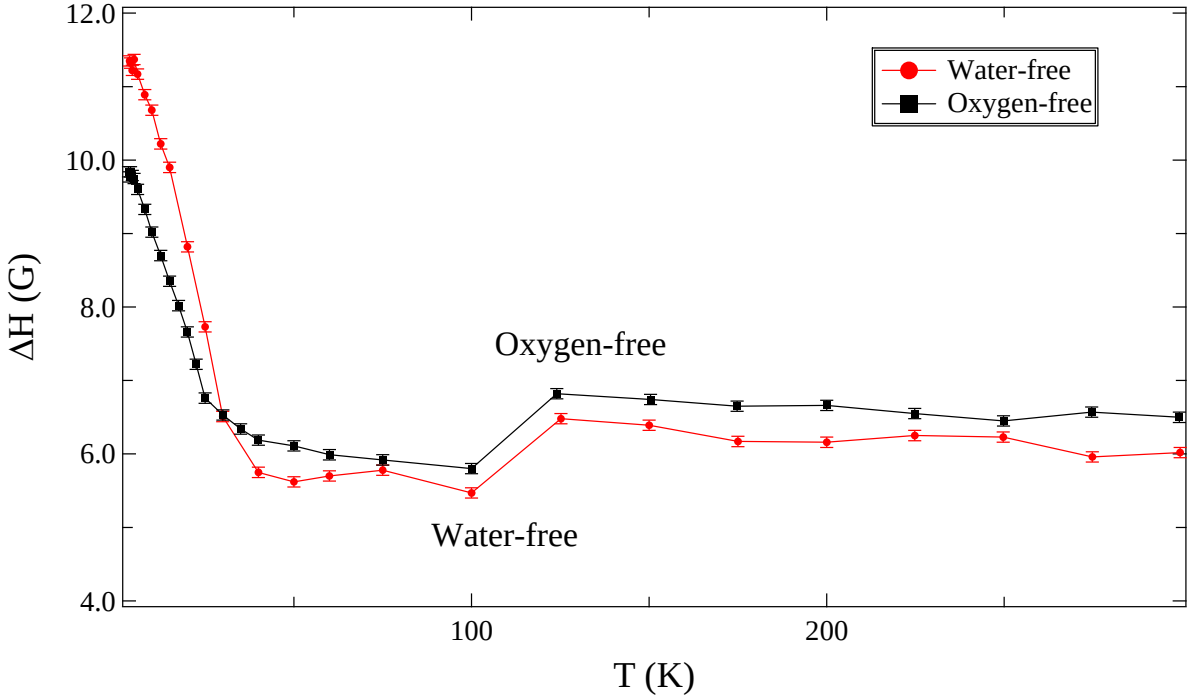

Figure 5. The linewidth of the Dysonian lineshape as a function of temperature for both sample conditions. The values for both the water-free and oxygen-free data clearly show linewidth motional narrowing.

The linewidth, ΔH, and dispersion to absorption ratio, α, can also tell us important information about spin dynamics. In Fig. 4, α is plotted versus temperature for both sample conditions. Whereas the water-free data stays relatively constant as a function of temperature, the oxygen-free data shows a consistent trend upwards with rising temperature, which implies that electron movement is increasing as the thermal energy rises. The temperature dependence of α for the oxygen-free condition may even show quasi-1D variable range hopping (VRH) behavior, although further analysis is necessary. One can directly test whether or not this conduction mode is being observed by measuring the DC conductivity as a function of temperature. We plan to perform this experiment within the next two months to compare to the temperature-dependent data for α.

As the thermal energy is removed from the system, electrons may hop between nanotubes less and less frequently. Not only does this affect the lineshape asymmetry, but also the linewidth. At low temperatures, the electron spin sees a relatively fixed dipolar field, which is the situation for any spin in a rigid lattice. When the thermal energy is increased, the spin sees less and less of the dipolar field because it is moving more. This movement causes the relaxation process to be less effective, producing longer spin lifetimes. Thus, at higher temperatures, the ESR lineshape has a narrower profile than at lower temperatures. This phenomenon, known as motional narrowing, has been observed in numerous systems with mobile spins [for a broad overview, see, e.g., N. Bloembergen *et al., Physical Review* **73**, 679 (1948)].

In Fig. 5, the observed linewidth versus temperature is shown for both sample conditions. Despite differences in magnitude and curve profile, both the water-free and oxygen-free data clearly show motional narrowing; this constitutes the first observation of this effect in nanotubes. The data in Fig. 5, along with data shown in Fig. 4, strongly suggest that the electron spin movement decreases as the temperature is lowered. Similar ESR findings have been reported in 1-D polymers [see, e.g., K. Holczer *et al., Phys. Rev. B* **23**, 1051 (1981) or V. Sitaram *et al., Physical Review B* **72**, 035209 (2005)]. In those studies, it was concluded that the spin movement (hopping) was between polymeric chains. In a similar manner, we postulate that the electrons are hopping between nanotubes.

Finally, power saturation studies were performed at selected temperatures for both the water-free and oxygen-free sample conditions. As Fig. 6 shows, we see an increase in the signal intensity up until ~6 mW, whereupon the signal begins to decrease. In addition, the Dysonian asymmetry changes once saturation begins. This observation suggests that the dispersion component of the spin susceptibility is not as strongly affected as the absorption component, which concurs with observations on many other systems. From the power saturation data, we hope to understand the population relaxation time, T_1, as a function of temperature and the evolution of the Dysonian curve as a function of both power and temperature.

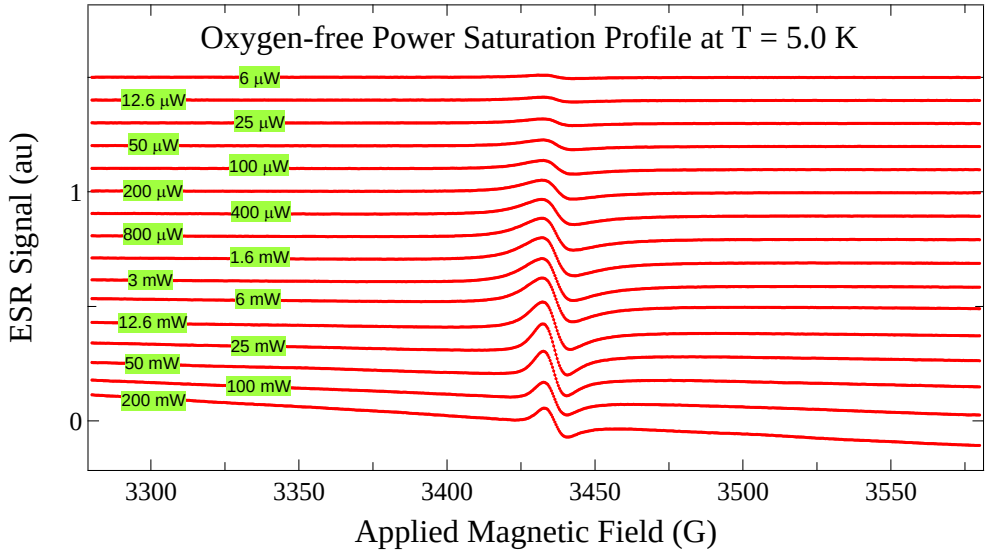

Figure 6. Power saturation ESR spectroscopy shows how the various lineshape parameters change as a function of power. Shown here is a power scan at 5.0 K for the oxygen-free sample condition. As expected, the signal intensity increases with increasing power until the absorption component becomes saturated. In this power scan, saturation occurs around 6 mW. Since dispersion typically saturates at much higher powers than absorption, a change in α is also observed at high powers.

Future

As previously mentioned, we are currently in the process of setting up a variable temperature and magnetic field DC conductivity system. By measuring the conductivity as a function of temperature for the water-free and oxygen-free sample conditions in nanotube films, we hope to understand more fully the conduction mechanism (electron transport) in nanotubes. This last experiment should be finished within the next two months. Once the DC conductivity work is done, a full analysis of the spin dynamics can be completed.

Module 2: Detection of Single Carbon Nanotube Electron Spin Resonance

Module 2 extends the work done on bulk SWNTs to the single nanotube level by using carbon nanotube-based field effect transistors (CNT-FET). The FET configuration shown in Fig. 7 presents two main advantages: first, it is the expected layout for spintronic and quantum processing applications, and second, the source and drain contacts permit a resistive detection of the electron spin resonance at different Fermi energies modulated by the gate. Moreover, this setup can directly compare charge and spin transport, which may allow spin-charge separation to be studied [see, e.g., Q. Si, *Physica C* **341,** 1519 (2000)].

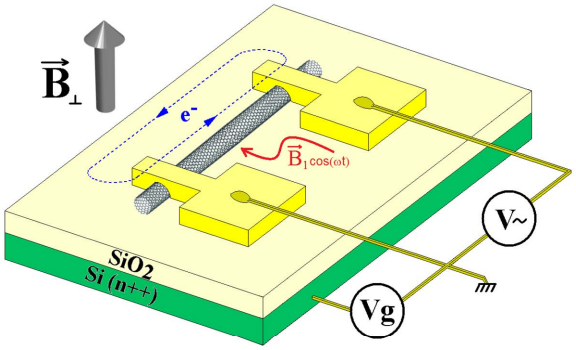

Figure 7. Experimental schematic for detection of single-tube ESR: a carbon nanotube is contacted by two electrodes (both source and drain are Au-Pd) used to apply a bias voltage [adapted from B. Raquet *et al., Phys. Rev. Lett.* **101,** 046803 (2008)]. The silicon substrate is used as a back gate, and the carbon nanotube is expected to be in the Fabry-Pérot regime (resonant, in blue). The excitations corresponding to the constant magnetic field and the microwave perturbing field are represented by a gray and red arrow, respectively.

Work accomplished

A process based on Rice University equipment has been developed to fabricate "home-made" CNT-FETs that suit the specific requirements of this experiment. Two avenues for producing CNT-FETs are currently being pursued. The first strategy consists of depositing HiPco nanotubes dispersed in an alcoholic solvent on a silicon substrate, on top of which a SiO_2 layer is thermally grown. Single nanotubes are then located by atomic force microscopy (AFM) (see Fig. 8) and contacted by e-beam lithography with lift-off, thus creating a short channel length, which allows us to achieve resonant electronic transport regimes at low temperature. Resonant phenomena, such as Coulomb blockade and Fabry-Pérot, are highly sensitive to any change or perturbation in the band structure and density of states under application of a magnetic field [see, e.g., J. Cao *et al., Phys. Rev. Lett.* **93**, 216803 (2004) or Kuemmeth *et al., Nature* **452**, 448 (2008)]. Thus, these probe configurations provide ideal detectors for even small changes caused by the microwave field. Moreover, the contacts are made of an alloy of gold and palladium in order to minimize the background signal from the electrodes; these two metals are

well known to provide the best contact quality with nanotubes. Such samples are in the process of being fabricated and are nearly complete.

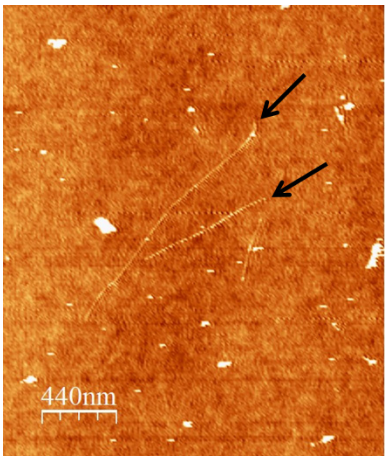

Figure 8. AFM image of two single nanotubes lying on SiO_2 (black arrows indicate the nanotube locations). The nanotube on the left has a measured diameter of d = 1.5±0.5 nm and will be contacted between two AuPd electrodes.

The second path for achieving single-tube ESR samples uses *in situ* CVD-grown nanotubes. This avenue would allow us to probe different types of nanotubes, while providing us with greater liberty to create different sample geometries. In particular, we could suspend a nanotube over a trench to avoid interactions with the oxide substrate and use longer channel lengths to reach more diffusive transport regimes.

Future Work

Preliminary tests will be done on the first samples within the next two months. In the next few weeks, standard transport characterization (resistance measurements) with respect to the source-drain and gate bias at room temperature will be performed. Metallic nanotubes will then be measured at low temperature (~4 K) to better characterize the transport regime. (These samples will be measured in collaboration with Professor Rui-Rui Du's Laboratory at Rice University.)

The next six months will consist of a more systematic study of the low-temperature ESR data. Measurements will be done in a Helium 3 cryostat (temperature range from 0.3 to 40 K) to probe the transport regimes described above and spin-charge separation. When a constant magnetic field $B_\perp$ is applied perpendicular to the nanotube axis, no changes in the electronic dispersion, and thus, in the charge transport pattern, is expected. Nevertheless, spin degeneracy will be lifted. A second magnetic field will be applied in the GHz frequency range as a perturbation field. When resonance is achieved, the spin population will be altered allowing us to directly probe spin transport. It is expected that different channel lengths (to tune through different diffusive regimes) and a variety of contact compositions (i.e., metal blends) will also be tested within the next six months.